International Journal on Magnetic Particle Imaging
Vol 3, No 1, Article ID 1703016, 9 Pages

Infinite Science Publishing

*Research Article*

# Towards the Integration of an MPI Compatible Ultrasound Transducer

Tim C. Kranemann*· Thomas Ersepke· Georg Schmitz

Chair for Medical Engineering, Ruhr-Universität Bochum, Bochum, Germany
*Corresponding author, email: tim.kranemann@rub.de

Received 25 November 2016; Accepted 25 February 2017; Published online 23 March 2017



**Abstract**

Magnetic particle imaging (MPI) is a tracer based modality and thus lacks anatomical information. Medical ultrasound (US) imaging provides the desired morphological data in real-time that could complement functional MPI images. However, most customary US devices will certainly be damaged by the strong alternating magnetic fields inside the MPI bore. Moreover, US equipment might degrade MPI signal quality. In this work, US components that are prone to eddy current heating were pointed out by presenting the major components of a medical US transducer. A theoretical model was utilized to derive maximum applicable sizes for conducting parts like electrode surfaces and cables. Heating experiments inside the MPI bore showed that heating can be managed by dispensing with extensive electric shields and keeping conducting structures reasonably small. Further, transducer dummies that were placed inside the MPI scanner bore and actively driven with US signals were used to assess the interferences between both modalities. The MPI signals showed a minor increase in the noise level when transducer dummies were present, while serious interferences were recognized when a dummy comprising a tuning inductor was electrically driven. The US signals showed strong disturbances in the frequency range of the MPI drive fields during MPI acquisition, which was decades lower than the relevant US frequency range. It is concluded that the combination of an MPI scanner and adapted US hardware is feasible. Future work needs to address the suppression of mutual interferences and their impact on image quality of both modalities.

## I. Introduction

Magnetic particle imaging (MPI) [1, 2] is a novel imaging technology which exploits the characteristics of superparamagnetic iron oxide nanoparticles and thus is a tracer-based modality. It generally lacks anatomical information and consequently an additional dataset is required to map the functional MPI data to the patient anatomy. For this purpose, magnetic resonance imaging has been used prior to an MPI acquisition and also the combination into a single dual-modality scanner [3] is investigated in order to perform MPI and MRI acquisitions in an intermittent mode.

Medical diagnostic ultrasound (US) [4–7] has been used for decades to image the mechanical properties of tissue and organs which reflect the morphological structure. US is appreciated for high patient safety, low cost, real-time capability and high spatial resolution. Performing US imaging inside the MPI scanner bore could be used to combine morphological US information with functional MPI data. This could be achieved in real-time and simultaneously with the MPI acquisition. However, since MPI utilizes strong, alternating magnetic fields and needs a low electrical interference environment, it is generally challenging to introduce any electronic component into the scanner bore.

Commercially available US systems have a multichannel transducer array located in a extensively

shielded scan head. The probes can comprise large electrode surfaces and usually further integrated electronic components, e. g., for electrical impedance matching. The probe is connected with a well-shielded multi-micro coaxial cable to a data acquisition unit with pulser-receiver electronics. On the one hand, in US components the magnetic fields of MPI cause heating due to eddy currents which can lead to rapid destruction. Moreover, it is to be determined if MPI induced signals harm the pulser-receiver electronics. On the other hand, currents on US cables or the nonlinear magnetization behavior of materials built in the probe might degrade MPI signals. These principal reasons prevent the insertion of standard US transducers into MPI scanners.

In this work, an overview of the basic requirements for an MPI compatible US system is given. Therefore, the major components of an US system are presented and evaluated regarding their compatibility to MPI. Since heating due to eddy currents is the major design challenge, theoretical back background is provided. After performing experiments in MPI, possible consequences on image quality with respect to both modalities are discussed. Thereby, heating of metallic components, the MPI compatibility of electrical matching elements, and the difference in signal-to-noise ratio due to mutual interferences is considered. The work concludes with design guidelines for critical components towards the integration of an US transducer into a preclinical MPI scanner.

## II. US Transducer Components

The MPI compatibility of an US device is determined by its internal construction. Fig. 1 shows a commercial 2.5 MHz 64-element phased array scan head cut though the axial/elevational plane. The depicted transducer can be subdivided into three major components: The transducer front, connections and tuning electronics, and cables for signal transfer with the acquisition system. These parts are discussed in the next subsections.

The basic level of compatibility of US and MPI is regarded as the prevention of damage when only one modality is active. An US transducer operating in an MPI scanner may hardly damage the MPI hardware severely since the electrical excitation can usually be incrementally increased to approach the operating currents cautiously. However, US transducers can instantaneously be destructed by the magnetic excitation- or drive-fields of an operating MPI scanner. These fields cause hysteresis and eddy current losses, both resulting in heating. While hysteresis losses can be avoided by the use of non-ferromagnetic materials like copper for all electrically conducting components, eddy current heating is the primary compatibility issue. In the scan head, all components are encased by a continuous circumferential copper shielding, see Fig. 1 (A). This continuous conducting surface is prone to eddy current heating and has to be dispensed in an MPI-compatible design.

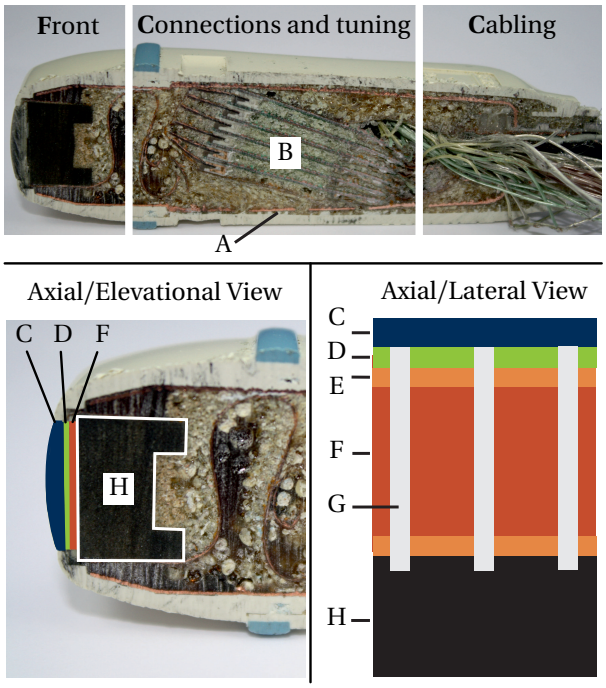


**Figure 1:** Top: Axial/elevational view of a through cut clinical US transducer. Bottom/left: Axial/elevational view of the transducer front. Bottom/right: Schematic of the transducer front in axial/lateral view. A – Circumferential copper shielding, B – Cable connections and electrical impedance matching, C – Acoustic lens, D – Acoustic matching layer, E – Electrodes, F – Piezo-electric material, G – Kerfs filled with composites for the separation of elements, H – Backing.

### II.I. Transducer Front

The transducer front contains the mechanically active components for transmitting and receiving ultrasonic waves. Modern 1-D array probes usually consist of 64–256 piezo-ceramic or piezo-composite [8] elements (F) that can operate as a phased array for steering and/or focusing the wavefronts. Therefore, they are mechanically and electrically separated by kerfs (G) filled with composite materials such as epoxy resin. A piezo-composite itself consists of a mixture of piezo-electric ceramics and plastics which both are not critical concerning eddy-current heating or magnetic losses. Metal film electrodes (E) usually made of gold or copper that are at maximum a few µm thin are attached to the piezo-elements at their front and back side. Via the electrodes, electric pulses excite the elements for transmission in the frequency range between 2-15 MHz for most US applications. For small animal imaging, systems in the range up to 50 MHz are available. With higher frequen-

10.18416/ijmpi.2017.1703016

cies, the size of the piezo-electric elements declines approximately inversely proportional.

Electrodes can either be attached to each element separately as depicted in Fig. 1 (E) or be connected on one side as a common (ground) electrode, which results in a large conducting surface. In [9] it is shown that a large electrode of a therapeutic US transducer shows strong heating in MPI. In this work, the impact of electrode sizes on eddy current losses is quantified and thin copper foils are experimentally examined.

A backing material (H) is usually attached to the backside of the piezo-elements to dampen the mechanical oscillation. Thereby, short pressure pulses can be transmitted which is required for high image resolution. The backing is dense and acoustically highly absorptive. Therefore, it may contain metal powder that is also beneficial for an adequate heat transfer [10] that arises in the piezo-material due to conversion losses.

The piezo-elements often reveal high acoustic impedances in comparison to the acoustic impedance of biological tissue, which leads to reflection of power at this interface. Thus, acoustic matching layers (D) are attached to the piezo-elements at the front side to maximize the transmission of acoustic energy into the medium. Matching layers are typically made from polymers. Layers with higher acoustic impedances can also be loaded with metal powders.

An acoustic lens (C) completes the transducer front for focusing of the waves in the elevational plane. The lens is typically made of silicon or rubber-like materials and is not critical with regard to heating. However, the MPI compatibility of each metal laden backing or matching material needs a specific individual evaluation which is beyond the scope of this contribution. Yet, since the metal powders are usually non-ferromagnetic and the composite is expected to be not electrically conducting, compatibility is anticipated.

### II.II. Electrical Impedance Matching

A high electrical impedance of the piezo-elements up to over 600 Ω [10] is determined by its material properties and size, as well as the effect of acoustic mass loading. Since the piezo-material with high electrical permittivity between the front and back electrode forms a capacitor, the impedance is highly capacitive [11]. The capacitive impedance of the connected coaxial cable also influences the overall impedance at the terminals to the acquisition system. Typically, for impedance matching, series or shunt inductors are placed as surface-mounted devices (SMD) directly in the scan head to cancel 40-60 % [10] of the element impedance to provide a good match to the $\approx 50-5000\,\Omega$ input impedance of the US acquisition system. Thereby, the electrical matching is an important measure for attaining a large bandwidth that is usually stated as a relative bandwidth $\frac{\Delta f}{f_c}$ in percent, where $\Delta f$ is the absolute bandwidth at −6 dB (different definitions exist) of the bandpass-shape round-trip spectrum around the center frequency $f_c$. While presumably most standard transducers have a relative bandwidth of 50-70 %, high quality probes achieve 100 % with an acceptable sensitivity through a sophisticated design process, including acoustical and electrical matching. The feasibility of electrical tuning in an MPI compatible design is here investigated experimentally.

### II.III. Cables

For the transfer of high voltage excitation pulses up to ca. 250 V to the transducer and transfer of low voltage receive signals (µV to mV range) to the acquisition system, typically a multi-micro coaxial cable is used which usually connects each piezo-element to one channel of the acquisition system. In [9] a 68×AWG 40 multi-micro coaxial cable with a silver plated copper braid shield was tested during a standard MPI imaging sequence. It is concluded that the dispense of the outer cable shield is essential to achieve MPI compatibility. In this work, the compatibility of cables of different diameters is analyzed by utilizing a theoretical model.

## III. Theory

To prevent the induction of destructive eddy currents, it is indispensable to avoid any conducting loop. Consequently, an ordinary continuous shielding of transducer components usually cannot be carried out in MPI compatible hardware. We consider a non-ferromagnetic infinitely long metal wire and a thin metallic plate of limited spatial extent, placed in a spatially homogeneous, quasi-stationary magnetic field, as idealized components to account for the two essential parts of every US transducer, i.e., cables and electrodes.

### III.I. Copper Wire

The generation of eddy currents in wires is extensively treated in [12] from which we report important results and universal considerations applicable to the problem at hand: Eddy current losses per unit length in a wire perpendicular to the magnetic field are therein calculated as

$$P_\perp = -\frac{2\pi}{\chi}\,|H|^2\,\varrho\left(\frac{r_0}{\delta}\right) \tag{1}$$

$$\varrho\left(\frac{r_0}{\delta}\right) = \mathrm{Re}\left\{\sqrt{2j}\,\frac{r_0}{\delta}\,\frac{\mathrm{J}_1\left(\sqrt{2j}\,\frac{r_0}{\delta}\right)}{\mathrm{J}_0\left(\sqrt{2j}\,\frac{r_0}{\delta}\right)}\right\}, \tag{2}$$

with the specific electrical conductivity $\chi$, the magnetic field strength amplitude $H$ ($[H]=\mathrm{Am}^{-1}$), and the radius of the wire $r_0$. $\mathrm{J}_0$ and $\mathrm{J}_1$ denote the zeroth and first order

Bessel function of the first kind and Re{} is the real part operator. The frequency dependent skin depth

$$\delta = \sqrt{\frac{2}{\omega \mu_0 \chi}}, \tag{3}$$

proves to be an important measure for many calculations on eddy currents, with the permeability of free space $\mu_0$ and the angular frequency $\omega = 2\pi f$ of the quasi-stationary magnetic field. For copper, $\delta = 425\,\mu\text{m}$ with $\chi = 561 \cdot 10^6\,\text{S m}^{-1}$ at a typical MPI drive field frequency of $f = 25\,\text{kHz}$.

The skin depth $\delta$ is a measure of the depth of magnetic field penetration in that eddy currents are concentrated due to the skin effect. For a wire of radius $r_0 \gg \delta$, the phenomenon of eddy currents is limited to its surface, while the inner wire remains eddy-current-free where no losses arise. In contrast, if $r_0 \ll \delta$, losses are generated more homogeneously in the volume of the wire. With the aid of the skin depth, (2) is approximated to

$$\varrho\left(\frac{r_0}{\delta}\right) \approx \begin{cases} \frac{1}{4}\left(\frac{r_0}{\delta}\right)^4 & , r_0 \ll \delta \\ \frac{r_0}{\delta} - \frac{1}{2} & , r_0 \gg \delta \end{cases}, \tag{4}$$

in order to emphasize the proportionality relations

$$P \sim \begin{cases} |H|^2\, r_0^4\, f^2 & , r_0 \ll \delta \\ |H|^2\, r_0 \sqrt{f} & , r_0 \gg \delta \end{cases}. \tag{5}$$

Despite the proportionality, naturally $P$ is always lower for smaller $H$, $r_0$, and $f$, as calculated with (1). Although heating is dependent on the specific thermal characteristics of the material and its environment, it is generally beneficial when eddy currents are not concentrated in the outer boundary of a component, causing the losses to be spatially concentrated. Therefore, one usually chooses the characteristic dimension $d = 2r_0 \ll \delta$ so that in practice $P \sim |H|^2\, d^4\, f^2$ holds. This serves as a guideline for component sizing ($d$) subject to the magnetic field characteristics ($H$, $f$).

For a magnetic field oriented parallel to a wire,

$$P_\parallel = -\frac{\pi}{\chi} |H|^2\, \varrho\left(\frac{r_0}{\delta}\right) = \frac{1}{2} P_\perp, \tag{6}$$

is the power loss per unit length as calculated in [12], which also follows relation (5). A wire passing through the middle of the MPI scanner bore is exposed to the orthogonal $x$-, $y$-, and $z$-drive fields that generate a Lissajous-trajectory for each image acquisition. Hence, we expect that the induced power due to the orthogonal fields, all oscillating with almost the same frequency, leads to a maximum possible power loss of $P = P_\parallel + 2P_\perp = 5P_\parallel$. The power loss $P$ for different radii, field strengths, and frequencies, around typical values in MPI is shown in Fig. 2. Since $P(H)$ and $P(f)$ are plotted for $r_0 = \delta$, all relations of (5) are apparent.

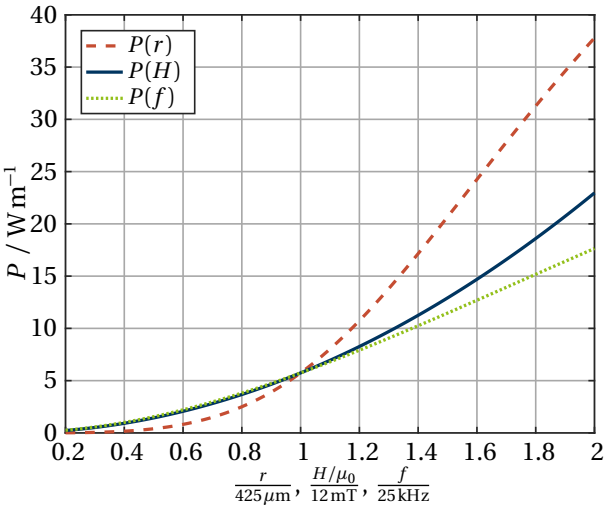


**Figure 2:** Power loss due to eddy currents in a copper wire of radius $r_0 = \delta = 425\,\mu\text{m}$ at $f_0 = 25\,\text{kHz}$ and $H_0/\mu_0 = 12\,\text{mT}$ over the normalized radius $P(r)$, magnetic field strength $P(H)$, and frequency $P(f)$. For $r \ll \delta$ losses are effectively reduced.

In practice, the heating associated with eddy current losses is most interesting, however, strongly dependent on the thermal characteristics of the component and its environment. If cooling due to radiation is neglected for objects with small surface area and relatively low temperature rise, a thermal equivalent circuit can be used to model the heating. For an isolated wire, the heat capacity of the conductor $C_\text{C}$ and of the insulation $C_\text{I}$, as well as the thermal resistance between the conductor and the insulation $R_\text{CI}$ is required. The heat transfer from the wire merely due to convection can be modeled as a thermal resistance $R_\text{I}$. However, if the conductor and the insulation is well connected $R_\text{CI} \approx 0$ and the overall thermal capacitance is $C = C_\text{C} + C_\text{I}$. For example, for a thin coated copper wire of $r_0 = 0.45\,\text{mm}$, with a specific heat capacity of $382\,\text{W s kg}^{-1}\,\text{K}^{-1}$, the heat capacity is calculated as $C_\text{C} = 2.17\,\text{W s K}^{-1}\,\text{m}^{-1}$. Presumably $C_\text{I}$ is much lower, hence, is neglected ($C \approx C_\text{C}$). Under this assumptions the simple model

$$\Delta T(t) = P\, R_\text{I}\left[1 - \exp\left(\tfrac{-t}{\tau}\right)\right], \quad t > 0, \tag{7}$$

can be applied to approximate the heating $\Delta T(t)$ over time $t$ with the thermal time constant $\tau = R_\text{I}\, C$.

## III.II. Thin Copper Plates

For thin copper plates, resembling electrodes, the same basic considerations apply and especially (5) holds when replacing the radius $r_0$ with $d = l/2$, half of the respective characteristic size. Analytical calculations for the dissipated power in thin plates of different shape are presented in [13]. There, an analytical approximation of

the total power dissipated in a rectangular plate is found

$$P \approx \frac{\pi^2}{8}\,\chi\, h\, \frac{a^3\, b^3}{a^2+b^2}\, f^2\, |B|^2 \tag{8}$$

$$= \frac{\pi^2}{4}\,\chi\, h\, l^4\, f^2\, |B|^2\,, \tag{9}$$

with the magnetic flux density amplitude $B = \mu_0 H$, the thickness of the plate $h \ll \delta$ and the rectangle dimensions $a$ and $b$ or the side length of a square $l$, respectively. While the warming of cables can often be well approximated by the aid of (7), for the heating of electrodes the more complex composition of surrounding materials, such as piezo-elements, backing or matching layers, are essentially determining the rate of heating. Hence, more specific and complex models are usually required.

# IV. Materials and Methods

## IV.I. Heating of Components

To evaluate heating, components were placed in a commercially available small animal MPI scanner (MPI 25/20 FF, Bruker BioSpin MRI, Ettlingen, Germany) and monitored with an IR thermography camera (VarioCAM, InfraTec, Dresden, Germany) from outside the scanner bore. For all experiments, the 25 kHz drive field strength was set to 12 mT for all (i.e., $x$, $y$, $z$) channels in the Bruker *ParaVision* software and the gradient field was turned off.

To test wires, twelve samples of copper wire with a thin polyimide coating (*i. a.* Dielektra Porz, Cologne, Germany) with a diameter between 0.15-1.5 mm were mounted on self made, round (≈ 85 mm diameter) paperboard carriers and placed in the middle of the 700 mm long scanner bore comprising a diameter of 119 mm. To evaluate the heating of thin electrodes, copper foils of 18 µm thickness (JTCHTE, Gould Electronics, Eichstetten, Germany) were cut into squares of 1-10 mm edge length and were examined in the same manner. Due to the placement of the carrier in the bore and of the samples on the carrier, some samples were positioned closer to the bore and the field generating coils.

It was accounted for the low emissivity of the thin coated shiny copper wires by adjusting the emissivity correction of the IR camera to a standard literature value of $\epsilon = 0.65$ [14] and by verifying the order of magnitude of heating with a comparison of polypropylene tape (57401, Tesa, Norderstedt, Germany) coated areas. For the heating of copper electrode samples, it was not aimed for a quantitative temperature measurement and only the detectability of heating > 4 K was investigated.

For evaluating the heating of ferromagnetic impedance matching elements, ten different inductive SMD parts of sizes 0603 (ca. 1.6 × 0.8 mm and different hight), 0805 (ca. 2 × 1.25 mm), 1206 (ca. 3.2 × 1.6 mm), as well as two through-hole technology inductors all together covering a range of 0.1-100 µH were glued on a single paperboard carrier and were IR monitored.

## IV.II. Interferences in MPI

To evaluate whether MPI images are affected by passive or active US components, two transducer dummies (TD) were manufactured, see Tab. 1. Micro-coaxial cables taken from an older 3.5 MHz scan head (Model 8339210L1001, Siemens, Germany) were considered as standard transducer cables. One of these cables of 800 µm outer diameter and 180 cm length was connected to each transducer dummy. TD-1 has no electrical connection between copper stripes mimicking the transducer electrodes and thereby mainly the cable capacitance is charged and discharged when actively driven. TD-2 comprises a capacitor in parallel with a resistor to imitate a capacitive piezo-electric element. To mimic electrical matching at the transducer inside the MPI bore, a SMD inductor was additionally installed in series. The samples were successively placed in the scanner bore. MPI measurements were conducted with an open terminated cable and with the cable connected to a one-channel US device (US.Box, Lecoeur Electronique, Chuelles, France) transmitting ≈ 25 ns long pulses with a repetition frequency of 1 kHz and maximum 230 V peak voltage to a TD to imitate US operation during MPI acquisition.

**Table 1:** Transducer dummies (TD) manufactured: TDs have a 35 µm thick copper array structure with an active area of 15 × 60 mm, but the longer dimension separated into $n$ elements to achieve thermal compatibility. The space between elements (kerf) is constantly 230 µm while the width $w$ is varied. TD-2 has SMD components soldered on the copper stripes to mimic the electrical impedance $Z$ of an US transducer and an impedance matching inductor. Nominal element values are $R = 860\,\Omega$, $C = 75$ pF, and $L = 27\,\mu$H.

| Dummy nr. | $n$ | $w$ / µm | $Z$ |
|---|---|---|---|
| **TD-1** | 106 | 340 | $\infty$ |
| **TD-2** | 38 | 1340 | $R \| C + L$ |

To investigate the effect of strong eddy currents on MPI spectra, a copper disc of 320 mm² surface area, 35 µm thick, on a printed circuit board (FR-4 material) was placed in the middle of the bore. During all experiments, the spectra of all channels are acquired using the *ParaVision* software.

## IV.III. Interferences in US

To measure the potential influence of MPI operation on US signals, the same TD samples were connected to an

 

oscilloscope (TDS3034C, Tektronix, Beaverton, OR) terminating the samples at 1 MΩ in AC-mode. Thereby, it was aimed for an US-system independent signal characterization. A time series of the sampled signal was stored and analyzed before and during MPI acquisition with all drive fields at 12 mT.

# V. Results

## V.I. Heating of Components

The IR temperature measurements were not used to assess the thermal MPI compatibility of all samples quantitatively, since the emissivity $\epsilon$ of the imaged surfaces was not experimentally determined and a discrepancy in $\epsilon$ has a considerable impact on the measurement. In addition, measured surfaces may reflect temperature radiation of the surroundings and bias the measurement. However, relevant heating was always detected and verified by simultaneous IR monitoring of the carrier and the tape partially sticked over the samples.

The well observable heating of a wire of 0.9 mm diameter was employed to verify the theoretical considerations made, see Fig. 3. The wire heated up over 55 K after 70 s on the paperboard carrier at an ambient temperature of 19 °C. The model of the form

$$\Delta\widehat{T}(t) = A\left[1-\exp\left(\frac{-t}{B}\right)\right], \tag{10}$$

see (7), was fitted to the measured curve, resulting in $A = 59\,\mathrm{K} = \widehat{P}\widehat{R}$ and $B = 18\,\mathrm{s} = \widehat{R}C$, where $\widehat{\cdot}$ denotes measured parameters. The heat capacity per meter was determined based on the geometry and the material parameters as $C = 2.17\,\mathrm{W\,s\,K^{-1}\,m^{-1}}$. According to the model, $\frac{C}{B} = 8.29\,\mathrm{m\,K\,W^{-1}} = \widehat{R}$ allowed the calculation of the *a priori* unknown thermal resistance. With the aid of (7), the induced power was calculated $\widehat{P} = 7.26\,\mathrm{W\,m^{-1}}$. The theoretical value was $P = 7.01\,\mathrm{W\,m^{-1}}$.

In the same setup, a wire of 0.6 mm diameter showed a warming of 12 K after 70 s. At wires with a diameter below 0.6 mm no significant heating was observed (< 4 K). Eventually, wires with a diameter below 0.48 mm did not stand out from of the background of the IR camera image, hence, heating was below the detection limit.

Regarding the heating of thin copper plates, no warming was observed for the copper foils of 1-2 mm side length. All other samples showed heating. The copper foil with 10 mm side length heated up to over 70 K after 80 s. With only the $y$- and $z$- channel operating with fields parallel to the plates, a heating lower than 4 K independent of the sample size was observed.

Concerning the open terminated inductors tested as possible impedance matching elements, SMD inductors of size lower than 1206 were heated < 4 K, while the through-hole devices were at 15 K after 25 s. At that time an overload of the MPI amplifiers has been recognized

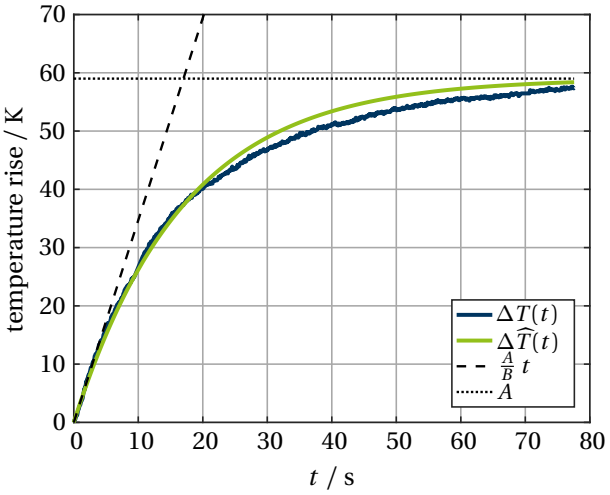


**Figure 3:** Temperature rise in a copper wire of 0.9 mm diameter in MPI fields with all drive field channels at 12 mT.

that has presumably existed since the beginning of the measurement. As a precaution, the drive fields were immediately turned off.

## V.II. Interferences in MPI

During all experiments, MPI spectra were recorded. Thereby, it was observed that merely the presence of TDs in the MPI bore did not change the received spectra conspicuously, see Tab. 2. Contrary, the carrier with multiple inductive elements with ferrite cores led to an (presumably instantaneous) overload in the MPI signals. Since the inductive elements were electrically not connected, the overload is ascribed to the magnetization characteristic of the ferrite material. Further, it was observed that a circular copper disk placed in the $y$-$z$-plane in the middle of the bore leads to a reduction of overall spectral energy of 14 dB, a decrease in the $y$- and $z$-channel and a slight increase in $x$-channel energy, see Tab. 2. Since the disk rapidly heats over 80 K, this effect is attributed to eddy currents, mainly induced by the $x$-direction drive field.

**Table 2:** Overall energy in the MPI spectra in dB (scaled in accordance to Fig. 4) for measurements with passive components. TD-1 does not influence the spectral energy. When eddy currents are present in the disk, energy is basically removed sample orientation dependent.

| sample | $x$-channel | $y$-channel | $z$-channel |
|---|---|---|---|
| empty bore | 99.5 | 103.4 | 96.3 |
| TD-1 | 99.6 | 103.5 | 96.4 |
| copper disk | 101.25 | 92.2 | 91.8 |

When US signals were sent to the TDs, MPI channels

were affected. The strongest effect was observed with TD-2, see Fig. 4b, that appears orientation dependent. However, also with TD-1 signals were induced in the $y$- and $z$-channels that were presumably more affected by a magnetic field of the coaxial cable that was orientated in $x$-direction. In addition, at TD-2 the axis of the inductive coil was oriented in $y$-direction.

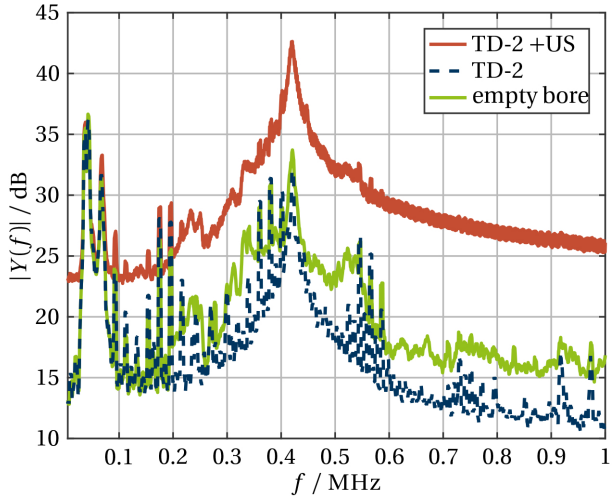


(a) Smoothed single acquisition $y$-channel spectra.

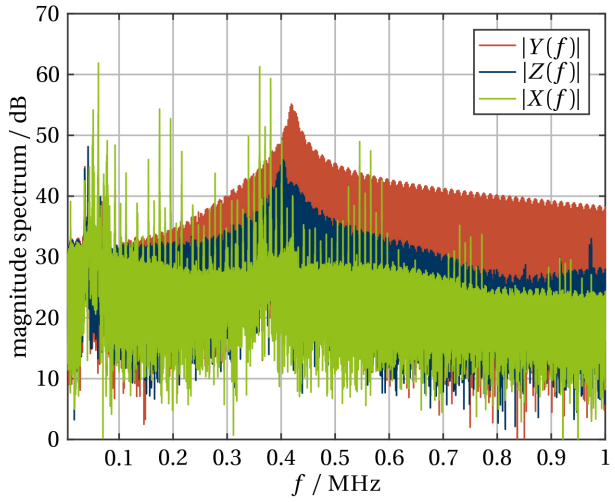


(b) All channel single acquisition spectra for TD-2 +US.

**Figure 4:** Magnitude of the MPI frequency spectrum, smoothed with a moving average filter of 100 taps or 460 Hz, acquired with TD-2 passive and actively driven (+US), compared with an empty bore measurement (a) and all channel non-smoothed spectra of actively driven TD-2 (b).

As depicted in Fig. 4a, TD-2 containing the inductive element increases the noise level about 10 dB compared to the reference measurement with an empty MPI bore. The spectra were, however, not changed by a passive TD-2. For TD-1, no significant change was observed. When the spectra were averaged over 1000 acquisitions, the interferences averaged out but the former characteristics of an empty bore spectrum did not recover.

### V.III. Interferences in US

Measurements of the induced voltage in the TDs and their cables were evaluated by taking a 2 ms acquisition of the oscilloscope signal with a sample rate of 25 MHz. Results are distilled in Tab. 3. Without MPI operation, the noise level was measured below −72 dBV in the frequency band of 1-5 MHz. The noise level increased when MPI was turned into acquisition mode. The same applies for the signal band of 23-27 kHz that covers the MPI drive field frequencies. In this range, a strong signal was measurable. The acquired signal over time for TD-1 is exemplary depicted in Fig. 5. When the TD cable was removed from the scanner bore, the induced signal rapidly decayed.

**Table 3:** Voltage induced into the US transducer cables connected to TDs. The signal power is calculated over the respective frequency band and values are reported in dBV.

| | no MPI operation | | all drive fields 12 mT | |
|---|---|---|---|---|
| | 23-27 kHz | 1-5 MHz | 23-27 kHz | 1-5 MHz |
| **TD-1** | −101 | −72 | −12 | −44 |
| **TD-2** | −107 | −73 | −10 | −48 |

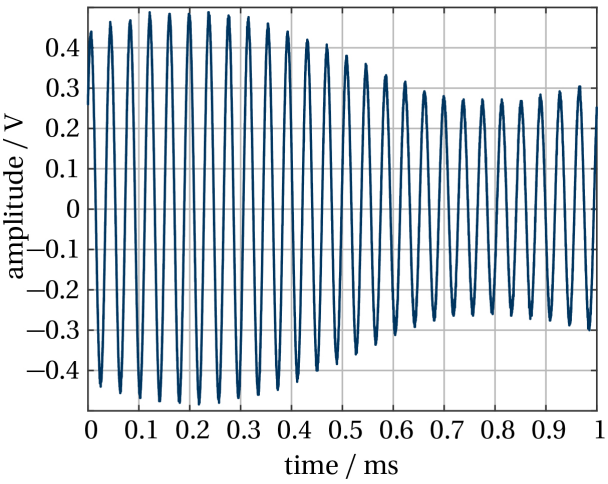


**Figure 5:** Induced voltage in the cable of TD-1 during MPI operation. The value of −12 dBV in the 23-27 kHz range stated in Tab. 3 translates into an amplitude of 355 mV.

## VI. Discussion

### VI.I. Heating of Components

For the design of electrodes and cables, a simple measure for the maximum possible structure size is desired.

Although heating is dependent on thermal rather than only the electrical characteristics, the skin depth (3) turns out to be a measure of importance. No heating is detected for wires of a diameter below $d < 0.48\,\mathrm{mm}$. Wires with $0.48\,\mathrm{mm} < d < 0.6\,\mathrm{mm}$ reveal low heating, possibly biased by the reflection of adjacent warmer wires. Further, no heating is detected with thin square plates of edge length $d < 1\,\mathrm{mm}$. Comparison of the characteristic sizes $d$ with twice the skin depth $2\delta = 850\,\mu\mathrm{m}$ shows that to avoid a significant heating, the characteristic sizes should be chosen smaller, i.e., $d < 2\delta$. More important, a homogeneous heating is presumably managed better than a strong and spatially concentrated. The proportionality relation (5) allows the estimation of applicable structure sizes of the examined geometries when field parameters change.

Calculation of the induced power loss based on the thermal measurement of one wire shows a deviation under 5 % to the theoretical model. Further, $\widehat{P}\widehat{R} = 58.1\,\mathrm{K} \approx A$ is also close to the measurement and can be regarded as a further verification. However, due to the position of the considered wire closer to the edge of the bore, a somewhat higher value was expected. For the laying of cables it is important to note that the field strength and heating generally increases towards the edge of the bore. Yet, the stationary temperature difference $\Delta\widehat{T}(t \to \infty) \sim P$ between a wire approximately in the middle of the bore and 50 mm from the middle of the bore was always less then 15 %. Consequently, to incorporate heating into the thermal calculations for an US transducer inside the bore, (1) and (8) can be applied.

The smaller inductive SMD parts tested do not show heating. They are not expected to carry induced currents when connected to a capacitive piezo-element, hence, the use of electrical matching is feasible with regard to thermal aspects. In summary, by a reduction of electrode surfaces to piezo-element dimensions and by the avoidance of continuous shields for cables and components, destructive heating can effectively be avoided.

## VI.II. Interferences in MPI

It was shown that the MPI signal is influenced by ferrite material of passive inductors up to a signal overload. Moreover, when TD-2 with a single SMD inductor is actively driven, MPI spectra are strongly distorted. This can be attributed to the leakage field of the inductor and currents on the imperfectly shielded cable. The latter is supported by the same but smaller influence of TD-1. However, although electrical impedance matching is often important for US bandwidth and sensitivity, it is expected to conflict with MPI requirements.

All interferences appear dependent on the orientation of the interfering source. For cables in $x$-direction, mainly $y$- and $z$-channels are influenced. Further, interferences are expected to increase with the magnitude of currents. Hence, for power transfer into the bore, higher voltages should be preferred and an adapted cable construction and installation in the bore can account for the spatial dependence of interferences.

The presence of strong eddy currents in the bore, that have basically the drive field frequency, does not change the MPI spectra in shape. However, they are detectable by a difference in overall spectral energy. This effect appears also dependent on the orientation of the sample that generates the induced interfering field. For lower eddy currents in adapted hardware, only a minor effect on MPI spectra is measurable.

Since the simple presence of components with reasonable structure sizes does not change the acquired MPI spectra conspicuously, it is expected that MPI operation can be performed when passive adapted US hardware is present. It is to be determined, if interferences of active components can be sufficiently suppressed by a dispense of inductive elements and averaging of multiple MPI acquisitions for one image. For the interpretation of the interferences due to US components, it has to be considered that with the TD experiments just one piezo-electric element was imitated, while a functional US transducer will usually comprise more than 64.

## VI.III. Interferences in US

Regarding US signal quality, the dispense of a shielding is usually detrimental for SNR. However, it can be accounted for narrow-band interferences in the MHz range inside the well shielded MPI cabin with digital filtering, when analog-digital converters are not overloaded by the induced voltages. Moreover, high-frequency shields can possibly be designed, that are not effective in the MPI but in the US frequency range.

The voltages measured on the US cables appear to be determined on the coaxial cable used. They are not significantly dependent on the TDs that have very different impedances and form slightly different induction loops. Since the induced voltages are relatively low (<1 V), this order of magnitude will neither harm pulser-receiver electronics nor piezo-elements. To prevent overloading during US acquisition, an electrical filtering of the kHz range signals might be necessary. This filtering, however, can potentially be provided by the high-pass characteristic of customary US front-end circuits so that signal quality is expected to be little affected.

The potential lack of an electrical impedance matching directly at the piezo-elements is considered as particularly detrimental for US signal quality. For example, the capacitance of a piezo-electric element is usually lower than 100 pF while the capacitance of a micro coaxial cable of 1 m length can have the same order of magnitude. This increases the quality factor of the overall electrical system which can never be fully recovered by broadband impedance matching techniques. A lim-

 

ited impedance matching, however, can be conducted directly outside the scanner bore.

## VII. Conclusion

Towards the integration of an US transducer into an MPI scanner, the heating due to MPI drive fields was examined as a primary compatibility issue. Therefore, a guideline for the determination of applicable structure sizes depending on drive field strength and frequency is given and equations for the calculation of remaining eddy current losses are stated. Accordingly, basic compatibility of US equipment is achieved by dispensing with continuous shielding and any induction loop, the reduction of electrode and cable sizes, as well as the use of non-ferromagnetic materials.

Further it is shown that the operation of US hardware inside the scanner bore affects MPI signals. Contrary, merely the presence of adapted US hardware does not necessarily degrade MPI image quality severely. A compromise, however, has to be made with regard to image quality of US when dispensing with electrical impedance matching inside the MPI scanner bore. At the same time MPI is expected be affected by the MHz currents on US cables. Nevertheless, it is potentially possible to acquire images with both modalities intermittently as well as simultaneously. Future experiments with compatible US hardware will provide quantitative results regarding the influence on image quality and the suppression of mutual interferences.

## Acknowledgement

This work was funded by the German Federal Ministry of Education and Research, contract number 13GW0069B (project SAMBA-PATI). The authors would like to thank Alexander Neumann and particularly Thomas Friedrich from SAMBA-PATI for MPI measurements.

## References

[1] B. Gleich and J. Weizenecker. Tomographic imaging using the nonlinear response of magnetic particles. *Nature*, 435(7046): 1214–1217, 2005. doi:10.1038/nature03808.

[2] T. Knopp and T. M. Buzug. *Magnetic Particle Imaging: An Introduction to Imaging Principles and Scanner Instrumentation*. Springer, Berlin/Heidelberg, 2012. doi:10.1007/978-3-642-04199-0.

[3] J. Franke, U. Heinen, H. Lehr, A. Weber, F. Jaspard, W. Ruhm, M. Heidenreich, and V. Schulz. System Characterization of a Highly Integrated Preclinical Hybrid MPI-MRI Scanner. *IEEE Trans. Med. Imag.*, 35(9):1993–2004, 2016. doi:10.1109/TMI.2016.2542041.

[4] B. A. J. Angelsen. *Ultrasound Imaging*. Emantec, Trondheim, 2000.

[5] P. N. T. Wells. Ultrasound Imaging. *Phys. Med. Biol.*, 51(13):R83, 2006. doi:10.1088/0031-9155/51/13/R06.

[6] K. K. Shung. *Diagnostic Ultrasound: Imaging and Blood Flow Measurements*. CRC Press, Boca Raton, 2006.

[7] T. L. Szabo. *Diagnostic Ultrasound Imaging: Inside Out*. Elsevier, Oxford, 2014.

[8] T. T. Wang, J. M. Herbert, and A. M. Glass. *The Applications of Ferroelectric Polymers*. Chapman and Hall, Glasgow, 1988.

[9] T. C. Kranemann, T. Ersepke, and G. Schmitz. Design of a Magnetic Particle Imaging Compatible HIFU Transducer Array. In *IEEE Int. Ultrasonics Symp.*, 2016. doi:10.1109/ULTSYM.2016.7728476.

[10] R. E. McKeighen. Design guidelines for medical ultrasonic arrays. In *SPIE Medical Imaging*, 1998. doi:10.1117/12.307992.

[11] G. S. Kino. *Acoustic Weaves: Devices, Imaging, and Analog Signal Processing*. Prentice-Hall, London, 1987.

[12] H. Kaden. *Wirbelströme und Schirmung in der Nachrichtentechnik*. Springer, Berlin/Heidelberg, 1959.

[13] N. J. Siakavellas. Two simple models for analytical calculation of eddy currents in thin conducting plates. *IEEE Trans. Magn.*, 33 (3):2245–2257, 1997. doi:10.1109/20.573839.

[14] OMEGA Engineering GmbH. Emissionsfaktoren. online. URL `www.omega.de/temperature/Z/pdf/z088-089-de.pdf`.

 